NANO LETTERS

2007
Vol. 7, No. 8
2395−2398

Nanoscale Oxide Patterning with Electron–Solid–Gas Reactions

Peter A. Crozier*

LeRoy Eyring Center for Solid State Science, School of Materials, Arizona State University, Tempe, Arizona 85287-1704

Received May 3, 2007; Revised Manuscript Received July 6, 2007

ABSTRACT

A novel nanoscale oxide patterning technique based on electron beam induced transformation in a gas environment is demonstrated. Localized phase transformation is induced in the surface region of a substrate, resulting in the formation of an oxide pattern that is embedded in the surface. The composition of the transformed region is determined only by the substrate and gas composition. The spatial resolution of the technique is about 15 nm.

The ability to create patterns of arbitrary shape on substrates of varying size and shape has huge potential in a wide range of fields from optoelectronics to biological applications. Many different direct write techniques have been developed to permit controlled nanoscale patterning with the most popular including optical lithography, e-beam lithography, focused ion beam, and nanoprinting technologies. Most of the patterning techniques involve deposition, etching, or deformation of material on the surface of a substrate. Recently, direct focused electron beam induced processing (FEBIP) methods have attracted renewed attention because of their simplicity and high spatial resolution as a result of new developments in instrumentation.[1−4] Depending on the type of precursor employed, the FEBIP results in either localized electron beam induced deposition (EBID) or localized electron beam induced etching (EBIE). Here we describe a novel form of FEBIP in which a localized phase transformation is induced, resulting in the formation of a nanoscale chemical pattern embedded in the surface of a substrate. This technique, which shall be called electron beam induced transformation (EBIT) to distinguish it from other forms of FEBIP, combines a subnanometer focused electron beam with a gas atmosphere to pattern materials at the nanometer level. Nanoscale oxide patterning on a substrate is accomplished simply through irradiating the region of interest with a subnanometer focused electron beam in an oxidizing atmosphere. This direct chemical transformation does not require any mask or development steps, and the resulting composition is determined solely by the substrate-gas interaction. The spatial resolution is 15 nm and the depth of the transformed region can be a few tens of nanometers. Moreover, such patterning can be performed on metals, ceramics, and semiconducting substrates of arbitrary shape. It can be used to pattern both rough and smooth surfaces and could be used to chemically functionalize existing nanostructures.

All the nanoscale processing described here was performed on an FEI Tecnai F20 environmental scanning transmission electron microscope (ESTEM).[3] This instrument has a differentially pumped environmental cell allowing gas pressures of up to 8 Torr in the vicinity of the TEM sample. The system is very versatile, and a wide range of different gases and CVD precursors have been successfully used to study materials nanofabrication based on electron beam induced deposition.[2,4,5] The instrument operates at 200 kV, and it has a field emission gun electron source that allows very intense electron probes down to 0.2 nm in size to be formed. The instrument can be operated in conventional broad beam TEM mode or in scanning mode (STEM) and is capable of yielding atomic resolution phase contrast bright-field TEM images and Z-contrast STEM images. It is fitted with a Gatan imaging filter, which allows nanometer resolution electron energy-loss spectroscopy and elemental mapping to be performed. The gas reaction cell, the small probe forming capability, and the powerful nanocharacterization capability make this instrument ideally suited for exploring and developing novel methods for nanoscale patterning.

Si_3N_4 substrates were selected for this experiment because they are normally relatively inert during electron irradiation under typical high vacuum conditions. This substrate is thus ideally suited to demonstrating nanoscale material changes induced when different gases are introduced to the environmental cell. Si_3N_4 membranes 30 nm in thickness (obtained from Ted Pella, Inc.) were loaded into a Gatan hot stage and inserted into the ESTEM. The films were subjected to an in situ cleaning step that typically consisted of heating to

* E-mail: crozier@asu.edu.

10.1021/nl071044+ CCC: $37.00
Published on Web 07/20/2007

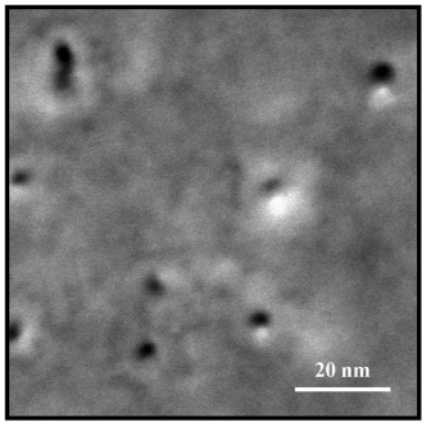

Figure 1. Z-contrast STEM image of randomly placed holes created in a Si_3N_4 substrate using focused electron beam etching in a H_2 atmosphere (holes are dark).

300 °C in flowing H_2 for 30−60 min to remove residual hydrocarbons and other undesirable species from the surface of the membrane. The films were then cooled to 150 °C before patterning. To create a local change in the substrate, gas was admitted to the environmental cell and the sub-nanometer electron beam positioned on the region of interest for a fixed period of time. The gas pressure was kept close to 0.5 Torr, and the electron beam current and diameter were 0.2 nA and 0.7 nm, respectively. In some cases, the electron beam was stepped over the substrate in a raster pattern to make periodic arrays of dots. The fabricated structures were characterized using Z-contrast imaging, bright-field TEM imaging, and energy-filtered imaging. To obtain more information in the various transformation processes, in situ time-resolved EELS was performed during the transformation process. Separate experiments were performed in vacuum, N_2, H_2, and H_2O in order to investigate the dependence of nanoscale patterning on the gas environment.

Initial experiments in the high vacuum of the microscope (10^{-7} Torr) demonstrated that the Si_3N_4 films used in the current experiment were relatively unreactive during exposures of up to 10 s with the focused electron beam. No changes were observed in either the substrate morphology or composition during electron irradiation. However, introduction of 0.5 Torr of either N_2 or H_2 resulted in immediate localized etching and hole drilling during electron irradiation. Figure 1 shows a typical series of 3−5 nm holes obtained in a H_2 atmosphere (similar results were obtained in N_2). Careful analysis of the images and corresponding spectra (not shown) demonstrated that the holes run through the entire thickness of the film and can be as small 1 nm in some cases. This shows that even relatively inert materials and gases can become highly reactive in the presence of a high-energy, focused electron beam. In this case, the gas molecules are ionized in the vicinity of the surface, becoming highly reactive and capable of etching with relative ease.

A completely different type of reaction takes place when an oxidizing gas is introduced to the cell, leading primarily to surface changes in the composition of the material in the vicinity of the electron beam. Figure 2 shows the variation in the local composition of the Si_3N_4 membrane as a function

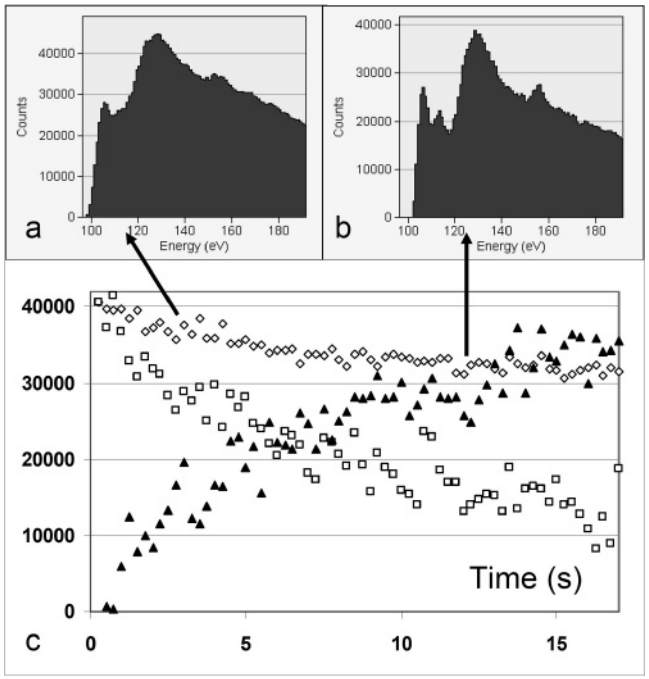

Figure 2. In situ Si L_{23} near-edge structure obtained during (a) 1 s and (b) 17 s irradiation in H_2O. (c) Variation in N (open squares), O (filled triangles), and Si (open diamonds) signals as a function of time derived from EELS during irradiation in H_2O. K-edges of O and N were used together with L_{23} edge of Si. Signals were scaled to reflect true change in elemental concentration.

of time recorded with in situ EELS during a 20 s electron irradiation in 0.4 Torr of water at 150 °C. Within the first 2 s of irradiation, the nitrogen content of the region falls by 25% with a corresponding rapid rise in the oxygen signal as a 3−4 nm thick layer on the upper and lower surfaces of the film gets rapidly converted to SiO_x. (Note that EELS measures the local projected composition through the entire film). After 18 s, 75% of the nitrogen has been removed from the irradiated area and most of the film has been converted to SiO_x. Some Si is also removed, showing that surface etching still takes place, but chemical transformation is the dominant process in this case. The near-edge structure of the Si L_{23} edge recorded with in situ EELS also shows the appearance of sharp characteristic peaks associated with the formation of SiO_x as the transformation proceeds.

The electron beam was then scanned in a raster pattern over the film to create a 10 × 10 periodic array of dots. Figure 3 shows the bright-field TEM image and a composite elemental map consisting of superimposed nitrogen and oxygen maps. The bright-field image (recorded with a large defocus to enhance the contrast from the transformed regions) shows a two-dimensional array of dots, and the corresponding elemental map clearly shows the presence of oxide dots embedded in the nitride matrix. Figure 3c is an oxygen line profile through a typical series of dots and shows the O concentration falling off with distance from the center of the dot with a full width half-maximum of about 15 nm.

Previous studies have also shown the ability of electron beams to facilitate oxidation processes on metal and semiconductors surfaces but at length scales measured in mil-

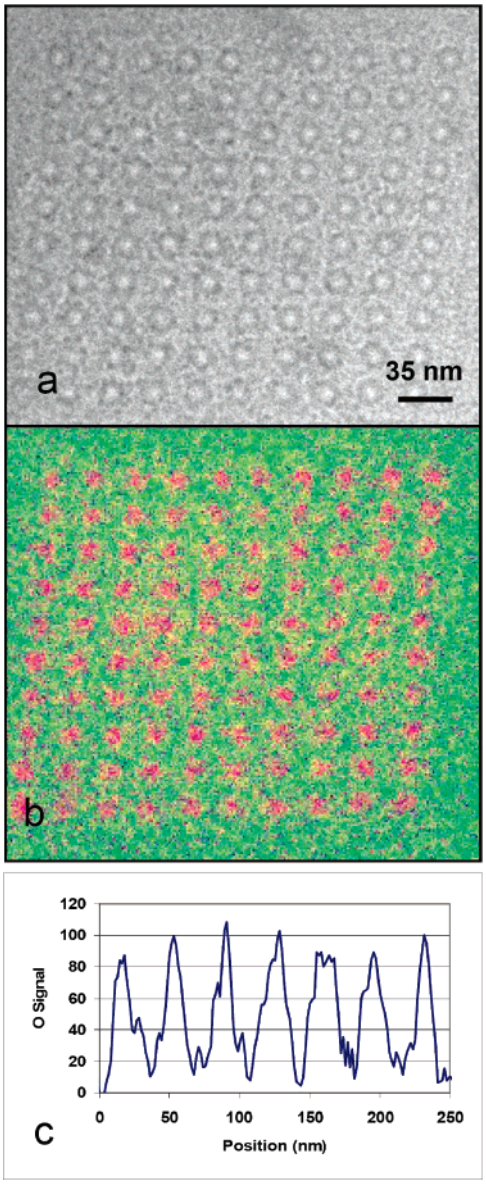

Figure 3. Array of SiO dots embedded in Si_3N_4 matrix via reaction between electron beam and H_2O. (a) Bright-field TEM image, (b) elemental map (red is O, green is N), and (c) O composition profile across several dots.

limeters rather than nanometers.[6,7] The reaction mechanism for localized phase transformation discussed here shares many common steps with these larger scale oxidation processes. However, the inherent length scales associated with some of the fundamental processes must be taken into account to understand the spatial distribution of the final phase for the current case. The critical processes in localized phase transformation are illustrated schematically in Figure 4a−c and involve the spatial distribution of fast secondary electrons, creation and diffusion of reactive surface species, and electron beam enhanced diffusion and mass removal within the reaction zone.

Even in the absence of electron bombardment, water molecules adsorbed on the Si_3N_4 surface may dissociate to form H^+ and OH^- species. Under electron irradiation, these species and many other species will form, leading to the production of highly reactive oxygen species.[6−9] The width of the surface reaction zone depends on the diffuse length of active oxygen species and the spatial extent of the electron flux through the surface. Secondary electrons emitted from the surface play a major role in molecular dissociation because their dissociation cross sections are much higher than the corresponding cross sections for high-energy primary electrons.[10−15] Consequently, the spatial distribution of secondary electrons leaving the surface imposes a lower limit on the size of the transformed area.

Developing an understanding of the spatial distribution of secondary electrons is not easy, but some qualitative insights can be gained by consideration of the energy dependence of both the electron mean free paths in solids and the dissociation cross sections. For simplicity, it can be assumed that, like the case for gas molecules, the dissociation cross section for the adsorbed water molecule has a maximum for electrons energies in the range 50−100 eV.[10] This effectively means that so-called fast secondary electrons (with energy greater than 50 eV) are primarily responsible for producing reactive oxygen species on the substrate surface. The approximate energy dependence of the mean free path for an electron traveling through a solid is well represented by the universal curves of Seah and Dench.[16] These curves show that the mean free paths for the secondary electrons of interest here are typically a nanometer or less. Momentum conservation results in the primary excitation events, leading to the generation of fast secondary electrons that travel mainly in the plane of the film for the high incident electron energy and low-energy transfers involved here.[9,10] The secondary electrons responsible for creating reactive surface species come from either this initial excitation event or are related to this event mainly through plural scattering, which partially preserves the directionality of the primary momentum transfer.

Figure 4a shows a likely schematic for dissociation events. Only those secondary electrons traveling close to the surface will participate in dissociation. Secondary electrons moving parallel to surface are likely to travel up to one mean free path from the primary beam before being scattered out of the surface. This suggests that the spatial extent of secondary emission will be on the order a few mean free paths on either side of the incident beam (i.e., a few nanometers). This simple argument has been supported by more rigorous Monte Carlo calculations for electron beam induced deposition.[17−20]

For EBIT, diffusion processes and mass removal will also influence the spatial extent of the transformation zone. The reactive dissociated fragments on the surface may diffuse outside the secondary electron generation region and substantially enlarge the reaction zone. In general, knock-on collisions by the primary electron beam will selectively impart more energy to the lighter N in the SiN film, making it easier to remove N than Si from the film.[21] The availability of reactive chemical species on the surface will result in selective removal of N from the surface region of the film. This will leave coordinatively unsaturated sites on the surface of the film that will readily bond with the reactive oxygen species, leading to the rapid formation of surface layers of

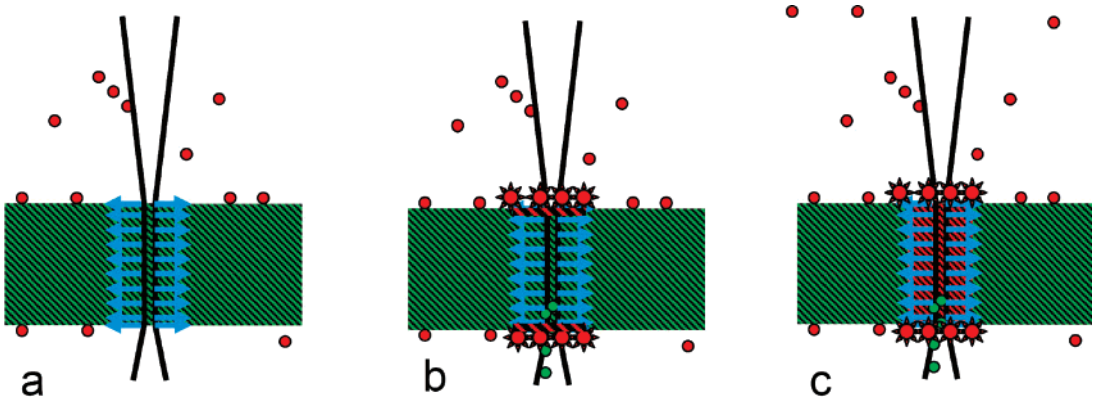

Figure 4. Schematic diagram illustrating the steps in nanoscale transformation. (a) Focused primary electron beam (black) irradiates the nitride sample (green shaded region) and generates secondary electrons (blue) that travel mostly in the plain of the foil. (b) Secondary electrons dissociate adsorbed water molecules (red circles) to create reactive oxygen species (red star). Nitrogen (green circles) is removed from reaction zone by primary beam/reactive species and an oxide layer forms on the surface (red shading). (c) Electron beam enhanced diffusion of oxygen takes place resulting in almost complete transformation from nitride to oxide (red shaded region).

SiO_x. In reality, both N and O may be continuously removed by the combined actions of the primary electron beam and the reactive species but O will be continuously replenished from the gas phase, effectively leading to the formation of an oxide layer on the surface.

Measurements of the full width half-maxima of the oxygen profiles suggest that diffusion processes effectively extend the reaction zone to a region about 7−8 nm in radius around the primary electron beam, giving a corresponding dot width of about 15 nm. A vertical oxygen concentration gradient will build up between the surface and the interior of the film and a lateral concentration gradient between the primary irradiated volume and the surrounding area. This will favor oxygen diffusing both from the surface into the bulk and also laterally away from the primary irradiated region. The rate of diffusion may be strongly enhanced by the generation of fast secondary electrons around the primary electron beam as it passes through the film. The zone of enhanced diffusion is similar to the reaction zone present in electron beam lithography and can be many mean free paths in width.[22,23] Recent calculations for high-energy electrons passing through a thin film show that 90% of the energy transferred to the surrounding species from fast secondary electrons occurs within 7 nm of the primary electron beam. This is in good agreement with the experimental radius of the reaction zone (7−8 nm) and suggests that fast secondary electron generation significantly influences the local diffusion process.

In summary, we have demonstrated that electron beam induced transformation is a novel method for accomplishing nanoscale oxide patterning on materials surfaces. The resolution of the technique is about 15 nm and is controlled by fast secondary electron generation and the diffusion lengths of reactive species. We have illustrated the method on a nitride ceramic, but results from the literature show that it should also work on semiconductors and metals. The composition of the induced chemical transformation is determine only by the substrate composition and reactive gas used for processing. The method is very simple, requiring only the introduction of water vapor, and can be applied to substrates of arbitrary shape and size. It should also be possible to fabricate other ceramics such as nitrides and carbides with a suitable choice of substrate and gas.

References

(1) Silvis-Cividjian, N.; Hagen, C. W. In *Advances in Imaging and Electron Physics*; Hawkes, P. W., Ed.; Academic Press: New York, 2006; Vol. 143, pp 1−235.
(2) van Dorp, W. F.; Someren, B.; Hagen, C. W.; Kruit, P.; Crozier, P. A. *Nano Lett.* **2005**, *5*, 1303−1307.
(3) Sharma, R.; Crozier, P. A.; Marx, R.; Weiss, K. *Microsc. Microanal.* **2003**, *9* (Supplement 02), 912.
(4) Crozier, P. A.; Tolle, J.; Kouvetakis, J.; Ritter, C. *Appl. Phys. Lett.* **2004**, *84*, 3441.
(5) Ketharanathan, S.; Sharma, R.; Crozier, P. A.; Drucker, J. S. *J. Vac. Sci. Technol., B* **2006**, *24*, 678.
(6) Bennett, S. L.; Williams, E. L. *Semicond. Sci. Technol.* **1991**, *6*, 1103.
(7) Ebinger, H. D.; Yates, J. T. *Phys. Rev. B* **1998**, *57*, 1976.
(8) Royall, C. P.; Thiel, B. L.; Donald, A. M. *J. Microsc.* **2001**, *204*, 185.
(9) Hill, M. A.; Smith, F. A. *Radiat. Phys. Chem.* **1994**, *43*, 265.
(10) Hwang, W.; Kim, Y.-K.; Rudd, M. E. *J. Chem. Phys.* **1996**, *104*, 1026.
(11) Inokuti, M. *Rev. Mod. Phys.* **1971**, *43*, 297.
(12) Egerton, R. F.; Malac, M. *Microsc. Microanal.* **2004**, *10* (Supplement 2), 1382.
(13) Li, W.; Joy, D. C. *J. Vac. Sci. Technol., A* **2006**, *24*, 431.
(14) Garand, E.; Rowntree, P. *J. Phys. Chem. B* **2005**, *109*, 12927.
(15) Sanche, L.; Parenteau, L. *J. Chem. Phys.* **1990**, *93*, 7476.
(16) Seah, M. P.; Dench, W. A. *Surf. Interface Anal.* **1979**, *1*, 2.
(17) Silvis-Cividjian, N.; Hagen, C. W.; Leunissen, L. H. A.; Kruit, P. *Microelectron. Eng.* **2002**, *61−62*, 693.
(18) Mitsuishi, K.; Liu, Z. Q.; Shimojo, M.; Han, M.; Furuya, K. *Ultramicroscopy* **2005**, *103*, 17.
(19) Silvis-Cividjian, N.; Hagen, C. W.; Kruit, P. *J. Appl. Phys.* **2005**, *98*, 084905.
(20) Hagen, C. W.; Silvis-Cividjian, N.; Kruit, P. *Scanning* **2006**, *28*, 204.
(21) Egerton, R. F.; Wang, F.; Crozier, P. A. *Microsc. Microanal.* **2006**, *12* (1), 65.
(22) Murata, K.; Kyser, D. F.; Ting, C. H. *J. Appl. Phys.* **1981**, *53*, 4396.
(23) Joy, D. C. *Microelectron. Eng.* **1983**, *1*, 103.

NL071044+